



Audio Engineering Society Convention Paper 10047

Presented at the 145th Convention
2018 October 17 – 20, New York, NY, USA

This convention paper was selected based on a submitted abstract and 750-word precis that have been peer reviewed by at least two qualified anonymous reviewers. The complete manuscript was not peer reviewed. This convention paper has been reproduced from the author's advance manuscript without editing, corrections, or consideration by the Review Board. The AES takes no responsibility for the contents. This paper is available in the AES E-Library (<http://www.aes.org/e-lib>), all rights reserved. Reproduction of this paper, or any portion thereof, is not permitted without direct permission from the Journal of the Audio Engineering Society.

An acoustic model of the Tapped Horn loudspeaker

Marco Berzborn^{1,2} and Michael Smithers³

¹Intern at Dolby Laboratories, San Francisco, USA (2016)

²Institute of Technical Acoustics, RWTH Aachen University, Aachen, Germany

³Dolby Laboratories, Sydney, Australia

Correspondence should be addressed to Michael Smithers (michael.smithers@dolby.com)

ABSTRACT

A lumped-parameter model of the Tapped Horn loudspeaker – a design where the loudspeaker driver radiates into the throat as well as the mouth of the horn simultaneously – is presented. The model enables the estimation of the far-field sound pressure response from the Thiele/Small parameters of the loudspeaker driver and an additional analytic two-port matrix representation of the Tapped Horn. Simulations, performed using the model for subwoofers, are compared to measurements from an actual loudspeaker.

1 Introduction

Horns have long been used to improve the efficiency of loudspeaker drivers by improving the impedance match between the loudspeaker driver and open air.

Traditional horns are fed energy from one side of the driver – the other side of the driver being enclosed in a sealed back volume. The Tapped Horn is a specific type of horn that uses energy from both sides of the driver. One side of the driver radiates energy into the throat of an expanding horn, whilst the other side of the driver radiates energy into the horn near the mouth or exit. The horn is usually short – typically one quarter of the longest wavelength and with significant reactive loading – and has a mouth diameter much smaller than the longest wavelength.

Due to the significant reactive loading of the Tapped Horn and its resonant natural horn response, obtaining a flat acoustic output involves a delicate balance of the drivers Thiele/Small parameters, horn dimensions, horn expansion rate, and feed or tap positions for both the front and rear of the driver into the horn.

The closed source software program HornResp [1], by David McBean, includes a Tapped Horn model and, in the authors experience, correlates well with the measured responses from physical builds. To further understand the Tapped Horn, the authors sought to simulate the acoustic performance of the Tapped Horn directly. Tappan [2] describes an analysis of the Jensen Transflex loudspeaker and gives insights into how to combine the responses of both the front and rear of the driver

into a basic equivalent circuit model. Beyond this, the authors are unaware of any publications describing the modeling of Tapped Horn loudspeakers.

This paper presents a equivalent circuit model of the Tapped Horn based on the driver's Thiele/Small parameters, and a two-port matrix representation of the horn. The paper briefly introduces the lumped-parameter model for an electrodynamic loudspeaker, derives an equivalent circuit horn model with an offset driver, and then derives a model for the Tapped Horn. Finally, comparisons between simulations and measurements from a physical prototype build are presented and discussed.

List of Common Symbols

Bl	Gyrator force factor
c	Speed of sound
C_{ms}	Mechanical compliance of spider and surround
f_s	Resonant frequency of the unmounted driver
F	Force on the moving mass of the driver
F_D	Force on the medium in front of the membrane
i	Electrical current
j	Imaginary unit
k	Wave number
L_e	Voice coil inductance
M_{ms}	Moving mass of the driver
ρ_0	Density of air
p_D	Pressure on the medium in front of the membrane
q_D	Volume velocity of the medium in front of the driver

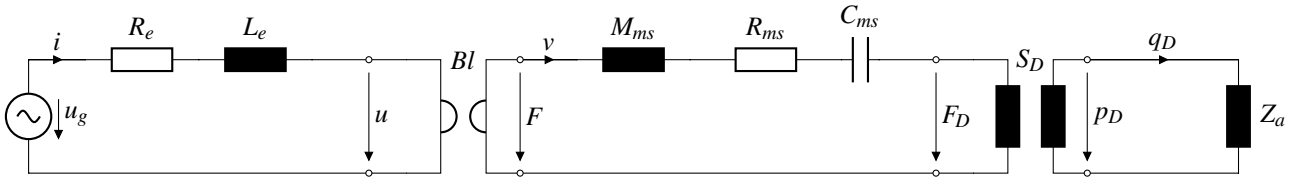


Fig. 1: Electrodynamic loudspeaker lumped-parameter model.

R_e	DC resistance of the voice coil
R_{ms}	Mechanical resistance due to friction losses
S_D	Surface area of the membrane
u	Back induced voltage
u_g	Source voltage
v	Voice coil velocity
Z_a	Impedance representing the acoustic load

2 A Simple Lumped-Parameter Loudspeaker Model

Before considering a horn model, it is useful to revisit the lumped-parameter model of a dynamic loudspeaker. Fig. 1 shows a equivalent circuit of an electrodynamic loudspeaker driver, as originally presented by Thiele [3, 4] and Small [5]. A gyrator of constant Bl couples the electrical and mechanical domains, and a transformer with constant S_D – the surface area of the membrane – couples the mechanical and acoustic domains. More details on the relations can be found in the literature [6, 7]. The electrical impedance of the loudspeaker driver is given as

$$Z_{ls} = \frac{u_g}{i} = Z_e + \frac{Bl^2}{Z_m + S_D^2 Z_a}, \quad (1)$$

where the impedance of the electrical circuit and the mechanical impedance are given as

$$Z_e = R_e + sL_e, \quad (2a)$$

$$Z_m = R_{ms} + sM_{ms} + \frac{1}{sC_{ms}}, \quad (2b)$$

and where Z_a is the complex acoustic impedance representing the acoustic load. The membrane velocity v can be derived from the voltage drop u over the gyrator as [8]

$$\frac{v}{u_g} = \frac{u}{u_g} \frac{1}{Bl} = \frac{1}{Bl} \frac{1}{1 + Z_e \frac{Z_m + S_D^2 Z_a}{Bl^2}}. \quad (3)$$

The volume velocity q_D , representing the moving air volume on the acoustic side, is then given as the product

$$q_D = S_D v. \quad (4)$$

3 Two-Port Representation of Horns

Horns can be modeled as acoustic transmission line elements [9, 10]. The relationship between the pressure p_v and the volume velocity q_v at the mouth of the horn, and the pressure

p_u and volume velocity q_u at the throat of the horn, can be expressed by the matrix product [9, 11]

$$\begin{bmatrix} p_u \\ q_u \end{bmatrix} = \begin{bmatrix} T_{11}^{\mu\nu} & T_{12}^{\mu\nu} \\ T_{21}^{\mu\nu} & T_{22}^{\mu\nu} \end{bmatrix} \cdot \begin{bmatrix} p_v \\ q_v \end{bmatrix}. \quad (5)$$

The matrix coefficients $T_{nm}^{\mu\nu}$ are dependent on the expansion rate of the horn, as well as the length of the horn segment $l_{\mu\nu}$, and the surface areas S_μ and S_ν of the throat and mouth, respectively. Analytic solutions for the case of one-dimensional horns can be found in the literature [9, 10]. The coefficients for the case of a horn with a parabolic expansion rate are given in Appendix A in Eqs. 22. Since the medium is homogeneous, reciprocity can be assumed and we can write [11, 12]

$$\begin{bmatrix} p_v \\ q_v \end{bmatrix} = \begin{bmatrix} G_{11}^{\mu\nu} & G_{12}^{\mu\nu} \\ G_{21}^{\mu\nu} & G_{22}^{\mu\nu} \end{bmatrix} \cdot \begin{bmatrix} p_u \\ q_u \end{bmatrix}, \quad (6)$$

with

$$\mathbf{G}_{\mu\nu} = \mathbf{T}_{\mu\nu}^{-1}. \quad (7)$$

Using Eq. 5 we can calculate the impedance into the throat of the horn as [6]

$$Z_r = \frac{p_u}{q_u} = \frac{T_{11}^{\mu\nu} \frac{p_v}{q_v} + T_{12}^{\mu\nu}}{T_{21}^{\mu\nu} \frac{p_v}{q_v} + T_{22}^{\mu\nu}} = \frac{T_{11}^{\mu\nu} Z_v + T_{12}^{\mu\nu}}{T_{21}^{\mu\nu} Z_v + T_{22}^{\mu\nu}}. \quad (8)$$

4 Model for a Horn with an Offset Driver

Fig. 3 depicts the case where the driver does not feed into the throat of the horn directly, but is mounted to the side of the horn at the cross-section with surface area S_1 . The throat of the horn is terminated by a rigid boundary with the surface area S_0 – the so called terminus. Consequently, this results in a volume velocity q_t into the terminus in parallel to the volume velocity q_1 into the middle horn section.

The terminus is modeled as an acoustical transmission line with an open circuit at its end (cf. Fig. 4); since at its rigid termination, the volume velocity has to vanish.

The equivalent impedance into the terminus is calculated as

$$Z_t = \frac{T_{11}^{10} Z + T_{12}^{10}}{T_{21}^{10} Z + T_{22}^{10}} \xrightarrow{Z \rightarrow \infty} \frac{T_{11}^{10}}{T_{21}^{10}}. \quad (9)$$

The equivalent impedance into the throat of the main horn section can be derived by inserting the radiation impedance for a vibrating piston in an infinite baffle [6] as the termination impedance into Eq. 8.

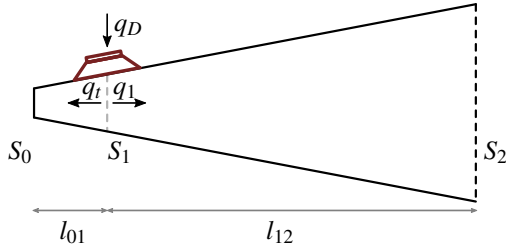


Fig. 3: Side view cross-section of a horn with an offset driver.

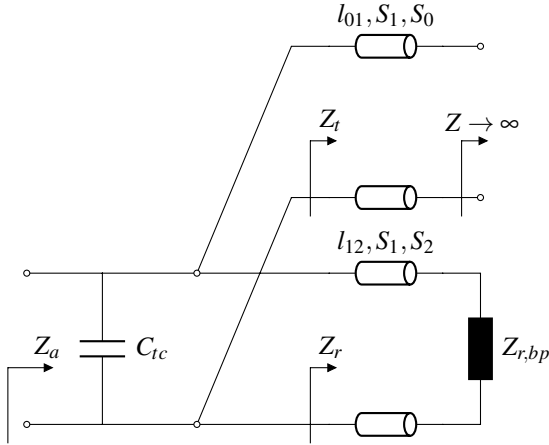


Fig. 4: Equivalent circuit diagram of a horn with an offset driver.

The radiation impedance of the complete horn Z_r' is then found as the parallel circuit comprising the radiation impedance of the horn section from the driver to the mouth Z_r and the terminus Z_t (cf. Fig 4),

$$Z_r' = \frac{Z_t Z_r}{Z_t + Z_r}. \quad (10)$$

The throat chamber in front of the driver is represented as a compliance [6, 7]

$$C_{tc} = \frac{V_{tc}}{\rho_0 c^2}, \quad (11)$$

in parallel to the radiation impedance, resulting in the full representation of the acoustic impedance Z_a of the horn cabinet (cf. Fig. 4) as [6]

$$Z_a = \frac{Z_r'}{1 + sC_{tc}Z_r'}. \quad (12)$$

Since the throat chamber compliance introduces a parallel circuit to the radiation impedance, the radiated volume velocity

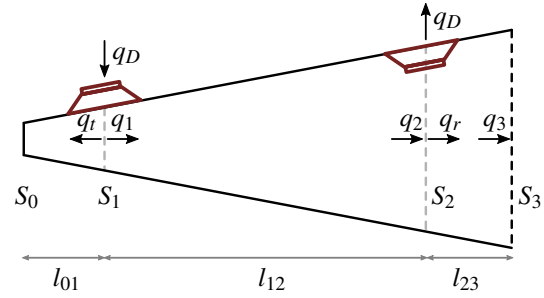


Fig. 5: Side view cross-section of the Tapped Horn.

is not equal to the volume velocity in front of the loudspeaker membrane.

5 The Tapped Horn

In the Tapped Horn cabinet, the rear of the driver is fed back into the mouth of the horn, which is typically achieved by folding the horn at least one time. A side view cross-section of a simple unfolded Tapped Horn cabinet is given in Fig. 5. The front of the driver generates a volume velocity q_D which results in a volume velocity q_1 into the throat of the middle segment of the horn and the volume velocity q_t into the terminus of the horn; analogously to the offset driver horn discussed in the previous section. Since the rear of the driver is fed back into the mouth of the middle horn segment the volume velocity q_r at the cross section S_2 in the horn is given as the sum of the volume velocity q_2 out of the main horn segment and the volume velocity $-q_D$ generated by the rear of the driver [2]. Consequently, we can derive two Kirchhoff node equations for the volume velocities at S_1 and S_2 :

$$q_D = q_1 + q_t, \quad (13a)$$

$$q_2 = q_D + q_r. \quad (13b)$$

The sketch in Fig. 5 can directly be transformed into an equivalent circuit diagram as given in Fig. 2. The complex impedance Z_t comprises the impedance of a transmission line with an open circuit termination. The complex impedance Z_r comprises the transmission line segment between cross sections S_2 , and S_3 as well as the radiation impedance of a vibrating piston in an infinite baffle; analogously to the horn with the offset driver (cf. Fig. 4). In case a throat chamber is introduced, an additional compliance is added in parallel to Z_t . This is easily modeled as an equivalent complex impedance combining Z_t and C_{tc} ,

$$Z_{t'} = \frac{Z_t}{1 + sC_{tc}Z_t} \quad (14)$$

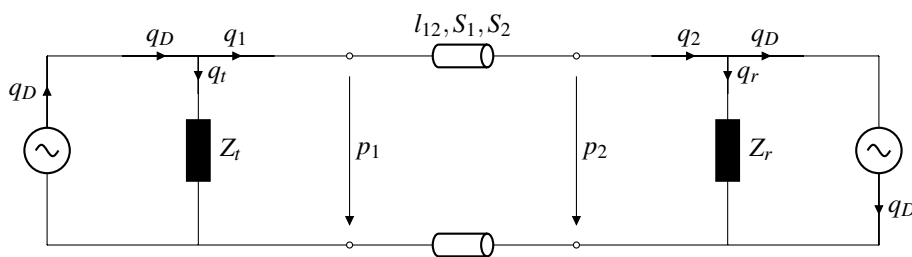


Fig. 2: Equivalent circuit of the tapped horn cabinet.

which replaces Z_t in Fig. 2.

In order to calculate the equivalent acoustic impedance of the enclosure Z_a , both the pressure at the front of the driver p_1 as well as the rear of the driver p_2 need to be considered. Consequently, the acoustic impedance is given as

$$Z_a = \frac{p_1}{q_D} + \frac{-p_2}{q_D}. \quad (15)$$

The pressures p_1 and p_2 can be written as

$$p_1 = Z_t q_t, \quad (16a)$$

$$p_2 = Z_r q_r. \quad (16b)$$

Combining Eqs. 13, 15, and 16 we can calculate the total acoustic impedance as

$$Z_a = Z_t \left(1 - \frac{q_1}{q_D} \right) + Z_r \left(1 - \frac{q_2}{q_D} \right). \quad (17)$$

The volume velocity relations $\frac{q_1}{q_D}$ and $\frac{q_2}{q_D}$ can be derived from Eqs. 13 and 16 and the matrix Eqs. 5 and 6 as

$$\frac{q_1}{q_D} = \frac{(T_{21}^{12} Z_r + T_{22}^{12}) G_{21}^{12} Z_t - T_{21}^{12} Z_r}{1 - (G_{22}^{12} - G_{21}^{12} Z_t) (T_{21}^{12} Z_r + T_{22}^{12})} \quad (18)$$

and

$$\frac{q_2}{q_D} = Z_t G_{21}^{12} + \frac{q_1}{q_D} (G_{22}^{12} - Z_t G_{21}^{12}). \quad (19)$$

It has to be noted that q_D can still be calculated using Eqs. 4, and 3 by substituting the corresponding acoustic impedance from Eq. 17. Finally, the volume velocity at the mouth of the horn q_3 is calculated using the two-port matrix coefficients of the horn segment l_{23} ,

$$q_3 = G_{21}^{23} p_2 + G_{22}^{23} q_r. \quad (20)$$

The radiated sound pressure in the far-field is then given as

$$p = -j \frac{\rho_0 c k}{2\pi r} q_3 e^{-jkr}. \quad (21)$$

6 Results

To validate the model, a sub-woofer cabinet was built using the B&C 18SW115-8 driver [13] - a driver known to perform well in horn loaded and Tapped Horn cabinet designs. The driver parameters are given in Table 1. Whilst commercial Tapped Horn designs often use multiple bends to give a compact design, this cabinet was built with a single fold, which was simpler to construct and ensured a predictable expansion rate through most of the horn.

Fig. 6 shows a side view cross-section of the internal acoustic path. The cabinet was constructed from 15 mm birch plywood with approximate outside dimensions - relative to the figure - of 1.81 m (width), 0.56 m (height) and 0.51 m (depth). The exterior rectangular volume - that is including the corner turn triangular spaces - was approximately 519 L. No absorption or padding was used in the cabinet and there was no throat chamber; the diameter of the hole in front of the driver was

Parameter	Value
f_s	32 Hz
S_D	0.121 m ²
Q_{ms}	5.6
V_{as}	0.187 m ³
M_{ms}	0.275 g
Bl	30.3 Tm
R_e	5.3 Ω
L_e	1.9 mH
C_{ms}	9.09×10^{-5} s ² /kg
R_{ms}	9.87 kg/s

Table 1: B&C 18SW115-8 parameters [13] (using $\rho_0 = 1.18$ kg/m³ and $c = 345$ m/s)

Parameter	Value
S_0	0.0190 m ²
S_1	0.0343 m ²
S_2	0.2104 m ²
S_3	0.2290 m ²
l_{01}	0.23 m
l_{12}	3.02 m
l_{23}	0.23 m
Horn expansion	Parabolic
Depth	0.479 m
Internal volume	Approx. 438 L

Table 2: Single fold Tapped Horn design parameters.

approximately the diameter of the outer edge of the driver surround. Table 2 shows the basic design parameters. It should be noted that since the horn expands in only one dimension, parabolic horn matrix coefficients were used in the model (see Appendix A).

Fig. 7 compares the far-field sound pressure response and Fig. 8 compares the electrical impedance. The result for the sound pressure shows good correlation up to about 200 Hz. Above 200 Hz it is obvious from the more distinct resonances in the model, that the physical build has more inherent damping. This effect is especially evident when studying the resonance peaks in the impedance from the model (cf. Fig. 8) which show a much higher quality factor compared to the measurement. This mismatch is due to the fact that the model does not consider any damping inside the horn. The measured sound pressure shows a faster low-frequency roll-off than the model due to the presence of a 18 dB/oct high-pass filter with a cutoff frequency of 25 Hz before the power amplifier. The measurement was taken outdoors at a distance of 10 m, and the measurement windowed at approximately 140 ms to eliminate a reflection from an adjacent building.

Interestingly, when comparing this and other builds using different drivers and design parameters, the lowest electrical impedance peak is always lower in frequency for the model than for the physical build. This doesn't appear as a significant difference in the far-field sound pressure. It is unclear why this difference in the impedance occurs.

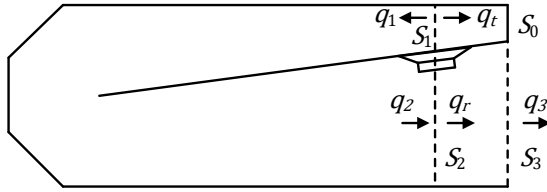


Fig. 6: Side view cross-section of the single fold Tapped Horn prototype.

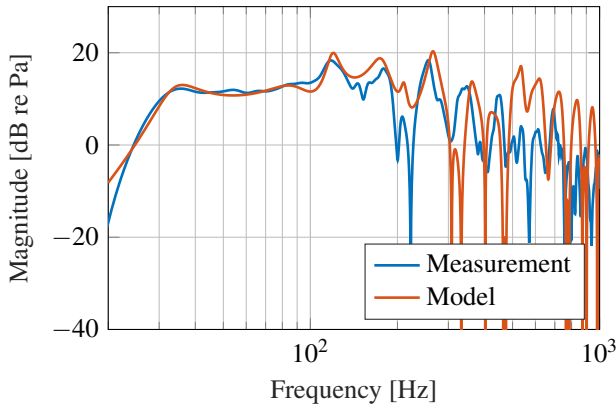


Fig. 7: Far-field relative sound pressure transfer function at a distance of 10 m and for an input voltage of 28.9 V_{rms}. Note that in the measurement, the excitation signal includes an 18 dB/oct high-pass filter with a cutoff at 25 Hz for displacement protection.

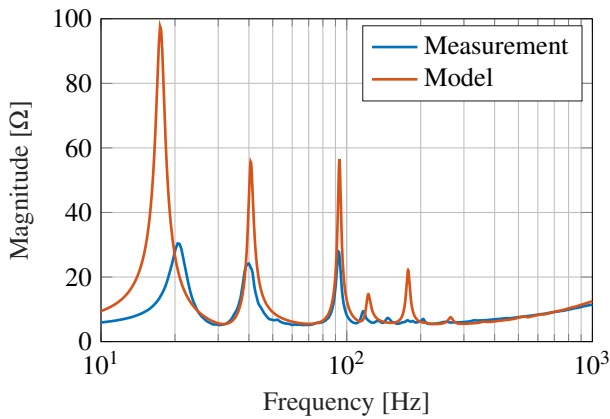


Fig. 8: Electrical impedance of the driver mounted in the Tapped Horn cabinet.

7 Discussion

The presented Tapped Horn model, in Figure 2, enables some insight into the relative contributions of the front and rear of the driver to the final frequency response.

Fig. 9 shows the amplitude and phase of the separate volume velocity components close to the rear of the driver. The volume velocity q_2 is the contribution from middle horn segment, whilst $-q_D$ is the contribution from the rear of the driver

(cf. Figs. 5 and 2). Finally, q_r is the sum of the two. From Fig. 9 it may fairly well be seen that q_2 dominates the velocity to the mouth of the horn at the fundamental eigenfrequency (around 32 Hz) of the horn, while the velocity of the driver is damped – therefore, limiting the membrane excursion as well. Above the fundamental eigenfrequency, q_2 and $-q_D$ are in phase, while their phase difference is π above the second eigenfrequency (73 Hz). This interference behavior significantly flattens the slope of the volume velocity flow towards the mouth of the horn q_r .

Fig. 10 shows how the separate volume velocities q_2 and $-q_D$ contribute to the sound pressure in the far-field – in 1 m distance for an input voltage of 1 V – denoted by p'_2 and p'_D , respectively. They are calculated analogously to Eqs. 20, and 21. It may easily be seen how the interference between the two volume velocities can be used to flatten the frequency response of the Tapped Horn cabinet.

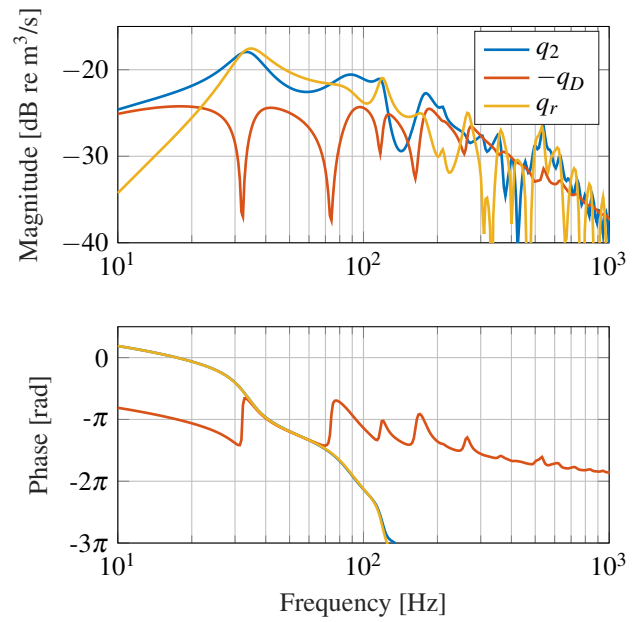


Fig. 9: Separated volume velocity transfer functions at the rear of the speaker at S_2 (cf. Fig. 5).

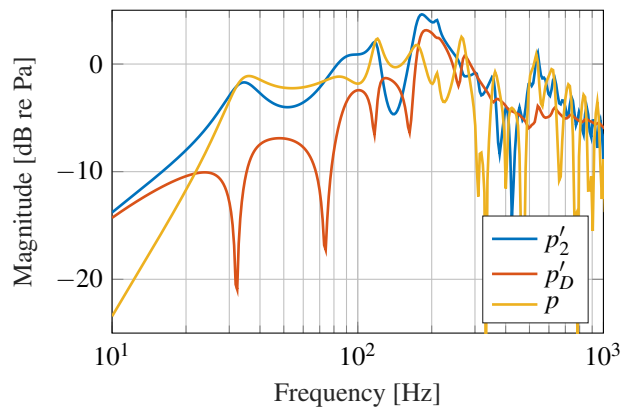


Fig. 10: Far-field sound pressure transfer functions derived from the separated volume velocities q_2 , q_D , and q_r , respectively.

8 Conclusion

Presented is a lumped-parameter model of the Tapped Horn loudspeaker cabinet. Simulated responses were compared to a physical build with a single fold and parabolic horn expansion. The modeled far-field pressure response correlates well with far-field measurements at low frequencies, both in absolute level and response shape. The modeled response shows a higher quality factor of resonances than in the physical build, caused by the lack of damping in the model.

Since the model uses an acoustic transmission line matrix expression for the horn expansion, different horn expansion equations - other than parabolic - can be used. Also, the horn can be further broken into multiple segments, each with different expansion rates and/or expansion equations, and the product of the matrices used within each of the three segments.

A Two-Port Matrices of Parabolic Horns

Solutions for the two-port matrix coefficients of different horn expansion rates are given in the literature [9, 10]. The coefficients for a horn with a parabolic expansion rate, used in the paper, are given as [9]

$$T_{11}^{\mu\nu} = \frac{x_\nu \pi k}{2} [J_1(kx_\nu) Y_0(kx_\mu) - Y_1(kx_\nu) J_0(kx_\mu)], \quad (22a)$$

$$T_{12}^{\mu\nu} = j \frac{x_\mu \pi k}{2} \frac{\rho_0 c}{S_\mu} [J_0(kx_\mu) Y_0(kx_\nu) - Y_0(kx_\mu) J_0(kx_\nu)], \quad (22b)$$

$$T_{21}^{\mu\nu} = j \frac{x_\nu \pi k}{2} \frac{\rho_0 c}{S_\mu} [J_1(kx_\mu) Y_1(kx_\nu) - Y_1(kx_\mu) J_1(kx_\nu)], \quad (22c)$$

$$T_{22}^{\mu\nu} = \frac{x_\mu \pi k}{2} [J_1(kx_\mu) Y_0(kx_\nu) - Y_1(kx_\mu) J_0(kx_\nu)], \quad (22d)$$

where S_μ and S_ν are the surface areas at the throat and the mouth of the horn, and $l_{\mu\nu}$ is the length of the horn. The distances x_μ and x_ν are the distances from the apex of the horn at $x = 0$ such that $l_{\mu\nu} = x_\nu - x_\mu$. $J_i(x)$ and $Y_i(x)$ are the i^{th} order Hankel functions of the first and second kind, respectively.

References

- [1] McBean, D. J., "HornResp Homepage," <http://www.hornresp.net/>, 2018, accessed on 2018-07-25.
- [2] Tappan, P. W., "Analysis of a Low-Frequency Loudspeaker System," *Journal of the Audio Engineering Society*, 7(1), pp. 38–46, 1959.
- [3] Thiele, N., "Loudspeakers in Vented Boxes: Part I," *Journal of the Audio Engineering Society*, 19(5), pp. 382–392, 1971.
- [4] Thiele, N., "Loudspeakers in Vented Boxes: Part II," *Journal of the Audio Engineering Society*, 19(5), pp. 471–483, 1971.
- [5] Small, R. H., "Closed-Box Loudspeaker Systems – Part I: Analysis," *J. Audio Eng. Soc.*, 20(10), pp. 798–808, 1972.
- [6] Olson, H. F., *Elements of Acoustical Engineering*, D. van Nostrand Company, Inc., second edition, 1957.
- [7] Beranek, L. L., *Acoustics*, McGraw-Hill: Electrical and Electronic Engineering Series, McGraw-Hill Book Company Inc., first edition, 1954.
- [8] Seidel, U. and Klippel, W., "Fast and Accurate Measurement of the Linear Transducer Parameters," in *Audio Engineering Society Convention 110*, 2001.
- [9] Mohammed, A., "Equivalent Circuits of Solid Horns Undergoing Longitudinal Vibrations," *The Journal of the Acoustical Society of America*, 38(5), pp. 862–866, 1965, doi:10.1121/1.1909817.
- [10] Mapes-Riordan, D., "Horn Modeling with Conical and Cylindrical Transmission Line Elements," in *Audio Engineering Society Convention 91*, 1991.
- [11] Makarski, M., *Tools for the Professional Development of Horn Loudspeakers*, Ph.D. thesis, RWTH Aachen University, Aachen, 2006, oCLC: 181578499.
- [12] Makarski, M., "Determining Two-Port Parameters of Horn Drivers Using Only Electrical Measurements," in *Audio Engineering Society Convention 116*, Berlin, 2004.
- [13] B&C Speakers s.p.a, "B&C 18SW115-8 Datasheet," 2018.